JCTC Journal of Chemical Theory and Computation

Article

Cite This: J. Chem. Theory Comput. 2019, 15, 5998−6009

pubs.acs.org/JCTC

Coupling Constants, High Spin, and Broken Symmetry States of Organic Radicals: an Assessment of the Molecules-in-Molecules Fragmentation-Based Method

Tumpa Sadhukhan, Daniel Beckett, Bishnu Thapa, and Krishnan Raghavachari*

Department of Chemistry, Indiana University, Bloomington, 47405 Indiana, United States

Supporting Information

ABSTRACT: We extend the application of our multilayer molecules-in-molecules (MIM) fragmentation-based method to the study of open-shell systems, particularly organic radicals. A test set of organic mono-, di- and polyradicals with a wide range in size, containing up to 360 atoms, was investigated. Total energies computed with MIM using density functional theory (DFT) were compared with full, unfragmented energies to assess the performance of MIM and to develop a systematic protocol for the treatment of large radical systems. More specifically, a two-layer (MIM2) model with a fragmentation scheme along the backbone involving covalently bonded dimers, trimers, or tetramers was considered, with DFT at a smaller basis set serving as the low level of theory. The MIM method was evaluated on the high-spin state and several possible broken-symmetry (BS) states for di- and polyradicals. When relevant spin−spin interactions were considered, the errors in total energies were less than 1 kcal mol^{-1}. In addition, the applicability of MIM2 was extended to predict the intersite magnetic exchange coupling constants (J), which were compared with reference values. Further, since the energy levels derived from Hamiltonian diagonalization are physically more meaningful, the calculated J values estimated from the BS-DFT methodology were used to obtain the lower spin state energies of the polyradicals. The difference in calculated total energies of the lower spin state between full and MIM2 lie within 1 kcal mol^{-1} in the majority of these cases. Our rigorous, quantum chemical study demonstrates that MIM can be successfully applied to the study of large organic radicals reliably and accurately within the framework of BS-DFT.

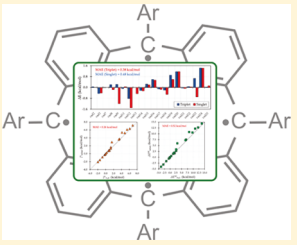

1. INTRODUCTION

Open-shell molecules (radicals) containing one or more unpaired electrons are known to be challenging systems to describe accurately with single-determinant-based electronic structure methods (including density functional theory). Functionally, they can exist in several possible spin states and routinely play key roles in electronic excited states. Radicals as a class tend to possess high energies, short lifetimes, and increased reactivity over more stable, closed-shell systems.[1] While commonly implicated as intermediates in organic, inorganic, and combustion-condition reactions due to their reactivity, many stable radical species are known to exist and find use in disparate fields of chemistry.[1] Stable, chemically useful radical species include spin clusters and organometallic luminaries such as carbenes, which play a major role in stabilizing metals in particularly high oxidation states.[2−4] Additionally, stable organic radicals serve as building blocks in organic magnetic materials[5−7] and in the development of spintronics.[8] They have been found to have properties desirable for spin transport and many spin filters employing organic diradicals have been proposed.[9−13] Over the years, experimental techniques, such as laser flash photolysis, electron spin resonance, photoelectron spectroscopy, and low-temperature matrix isolation infrared spectroscopy, have been developed and applied to the characterization of radicals.[14] However, as radical species are notoriously difficult to isolate, experimental techniques can only provide a piece of the puzzle and quantum chemical calculations have proven to be an invaluable tool for studying the electronic properties of open-shell molecules.[14]

In recent years, interest has grown in organic radicals with abnormally high spin states due to their high magnetic susceptibilities, bistability, biocompatibility, and low density.[15] Organic molecules possessing high multiplicity ground states also provide insight into how molecular structure affects spin interactions, giving us insight into the physical effects of electron spin. For example, only a small number of diradicals have been isolated with both strong ferromagnetic interactions between unpaired electrons and a thermally accessible singlet−triplet energy gap (ΔE_{ST}) on the order of thermal energy at room temperature (~0.6 kcal mol^{-1}).[16−26]

Ideally, ab initio multireference methods would be used to describe open-shell systems due to the problems of delocalization, spin contamination, and symmetry breaking present in the single-determinant Hartree−Fock (HF) or density functional theory (DFT) treatment.[27−34] Unfortunately, multireference methods are highly expensive for medium to large molecules even with relatively modest basis sets so single-reference DFT and wave function methods are likely to be used for the foreseeable future. Thus, it is immediately important to increase the applicability and reduce

Received: June 6, 2019
Published: October 18, 2019

Downloaded via INDIANA UNIV BLOOMINGTON on June 2, 2020 at 14:47:28 (UTC).
See https://pubs.acs.org/sharingguidelines for options on how to legitimately share published articles.

© 2019 American Chemical Society

DOI: 10.1021/acs.jctc.9b00563
J. Chem. Theory Comput. 2019, 15, 5998−6009

the scaling of more accurate single-determinant treatments.[35] Open-shell systems are studied with both unrestricted Hartree−Fock (UHF) wave functions or restricted open-shell Hartree−Fock (ROHF) theory. While ROHF wave functions have been shown to perform better as a reference for single-determinant wave function theory methods, such as MP2 and CCSD(T),[36] unrestricted wave functions find extensive applications with DFT.[37] While spin-contamination effects plague UHF wave functions, unrestricted density functional theory is less prone to spin contamination than UHF.[38] While both unrestricted and restricted versions of DFT have been used to derive radical stabilization energies,[39,40] it has been argued that spin contamination in the Kohn−Sham wave function is a feature rather than a fault and does not need to be eliminated.[41] Additionally, in the case of diradical species, unrestricted formulations have proven to be quite effective in obtaining reliable geometries.[42,43]

Nevertheless, regardless of the reference wave function, it is clear that large radical species require a balanced treatment, often involving multiple calculations to obtain di- and polyradical coupling constants. One of the most efficient and reliable ways to study large molecules that has arisen in recent years is the fragmentation-based[44,45] methodology in which the desired property of a large system is described by the properties of small fragments summed in some manner. A wide range of fragmentation-based methods has been developed by different research groups over the decades and these differ by the manner of fragmentation, the nature of the expression by which fragment properties are collected, and whether multiple levels of theory are employed or not.[44−46] Over the past few years, we have developed and applied the multilayer molecules-in-molecules (MIM) fragmentation method to a variety of systems, including water clusters and large biomolecules.[47−53] While MIM has been applied to a diverse set of systems, previous applications have been exclusively on closed-shell systems. The question of how to successfully fragment open-shell molecules while maintaining the correct spin state for the parent molecule is open-ended and largely unaddressed by the fragmentation community. Recent work has been done with a divide-and-conquer inspired method, demonstrating successful fragmentation and recovery of open-shell species through the localization of fragment molecular orbitals.[54] Additionally, the fragment molecular orbital fragmentation-based method has been extended to open-shell systems but has generally been restricted to monoradicals and the calculation of spin densities.[55,56] Here, we are interested not just in the behavior of a single radical site but in assessing the performance of an energy-based fragmentation scheme in computing coupling constants and the broken symmetry states of polyradicals.

Herein, we present the first application of the MIM energy-based fragmentation method to the study of open-shell systems. First, we have selected a range of small to medium-sized experimentally known and stable organic monoradicals to analyze if their energies can be reproduced by MIM through comparison to full (unfragmented) energies obtained at a target high level of theory. Next, we consider a set of stable organic diradicals to compare the performance of MIM relative to the full calculation, as well as available experimental results, in terms of both low- and high-spin energies, singlet−triplet gaps, and coupling constants. We have also included organic polyradicals possessing unusually high spin states to validate the performance of MIM on truly complex and large open-shell systems. Lastly, we report intersite magnetic exchange coupling constants and compare MIM to the full calculation of the energies of the lower polyradical spin states through diagonalization of the Heisenberg−Dirac−van Vleck Hamiltonian (HDvV).

2. COMPUTATIONAL METHODS

2.1. Molecules-in-Molecules (MIM) Protocol. The molecules-in-molecules (MIM) fragmentation method has been described in detail in previous papers; only the essentials will be described here and we refer the reader to previous work.[48−50,52] Throughout this study, we use a two-layer MIM model (referred to as MIM2), as shown in eq 1. Here, the energy of the full, unfragmented molecule is calculated at the low level of theory (E^{R}_{low}) and the fragmented energy is obtained at both the low (E^{r}_{low}) and (E^{r}_{high}) high levels of theory. The superscript 'R' refers to the full, unaltered system, whereas the superscript 'r' refers to energies obtained through the fragmentation approach. The energy of the fragmented molecule is treated in a generalized manner analogous to the model system in the ONIOM methodology of Morokuma and co-workers[57,58] with the low level energy subtracted out and the high level added in as an extrapolation to the energy of the full molecule calculated at the high level of theory

$$E^{MIM2} = E^{R}_{low} - E^{r}_{low} + E^{r}_{high} \quad (1)$$

To obtain the fragmented energies, E^{r}_{low} and E^{r}_{high}, we first cut single bonds between two nonhydrogen atoms to specify nonoverlapping, primitive monomers. Conjugated rings and *t*-butyl group are kept intact and not broken in the initial fragmentation procedure. Moreover, the fragmentation of bonds that would replace one center with two link atoms (i.e., in rings) is not carried out to avoid unphysical artifacts.[48] Local interactions between primitive monomers yield overlapping primary subsystems based on some prescription. In our case, we employ a number-based scheme wherein covalently bonded monomers are grouped into subsystems of η monomers. We explore dimer (η = 2), trimer (η = 3), and tetramer (η = 4) schemes in this work. Derivative subsystems are formed from the overlap of primary subsystems to avoid overcounting through application of the inclusion−exclusion principle during property summation. Calculations are performed on the derivative and primary subsystems with hydrogen link atoms to satisfy the valences of cut bonds. In an energy calculation step, the energies of each subsystem (primary and derivative) are obtained and summed according to the inclusion−exclusion principle. Calculations are performed at both the high and low levels of theory to obtain E^{r}_{high} and E^{r}_{low}, respectively, and the difference between them contributes to the MIM2 energy, as shown above in eq 1. To treat open-shell molecules, when nonoverlapping monomers are combined to form subsystems, the spin state of the subsystems depends on the number of radical centers for each monomer and their set spins. The user specifies atomic centers and their associated spin value as a list and fragment monomers containing the specified atoms are given an overall spin through summation. This same process is used to find the total spin for a subsystem (the actual units that calculations are performed upon). The multiplicity of each primary and derivative subsystem depends on the presence and number of radical centers in the subsystem. A representative example

DOI: 10.1021/acs.jctc.9b00563
J. Chem. Theory Comput. 2019, 15, 5998−6009

has been presented in Figure S1 of the Supporting Information.

2.2. Treatment of Radical Species. While a monoradical ($S = 1/2$) exists in the doublet (D) ground state, a diradical can exhibit either a triplet (T, high-spin, $S = 1$) or singlet (S, low-spin, $S = 0$) state. The magnetic exchange coupling constant, J, describes the degree to which two spins interact with each other. A positive J value corresponds to ferromagnetically coupled electrons and the highest spin ground state, whereas an antiferromagnetic interaction yields a negative J and a ground state of the lowest S value. For the triplet state, $E(\mathrm{T}) = -J/2$, whereas the singlet state energy is expressed as $E(\mathrm{S}) = 3J/2$. In the case of a triradical, the two possible states are either a doublet ($S = 1/2$ with $E(\mathrm{D}) = 2J$) or a quartet ($S = 3/2$ with $E(\mathrm{Q}) = -J$), neglecting coupling between disconnected sites. Thus, the magnetic exchange coupling constant can be calculated from the low-spin (LS)—high-spin (HS) energy gap.

$$J_{\mathrm{diradical}} = \frac{1}{2}[E(S=0) - E(S=1)],$$

$$J_{\mathrm{triradical}} = \frac{1}{3}[E(S=1/2) - E(S=3/2)] \quad (2)$$

To use eq 2, we need the energy of both the low- and high-spin states. However, the determination of an accurate $E(\mathrm{LS})$ is a challenging problem.

While multiconfigurational methods based on restricted open-shell treatments have been used successfully in some diradicals,[59] reasonable molecular geometries, relative energies, and spin polarization can be obtained from unrestricted density functional theory calculations at a reduced computational cost. The drawback to single-determinant, unrestricted methods is that only the highest spin state can be represented correctly. To overcome this problem, Noodleman and coworkers proposed the broken symmetry (BS) methodology in the framework of unrestricted DFT to calculate the coupling constant.[60−63] The lower spin states are a linear combination of these BS wave functions, which cannot be obtained directly from single-determinant DFT calculations. These BS determinants are not pure spin states; they possess an m_s value but no well-defined S quantum number. For a pure diradical, the ideal BS state is an equal mixture of the low- and high-spin states with $\langle \mathbf{S}^2 \rangle = 1$. A generalized formula to obtain coupling constants for diradicals was proposed by Yamaguchi et al.[64,65] in which the energy difference is corrected for the effect of spin contamination by scaling with the calculated $\langle \mathbf{S}^2 \rangle$ values.

$$J^{\mathrm{Y}} = \frac{(E_{\mathrm{BS}} - E_{\mathrm{HS}})}{(\langle \mathbf{S}^2 \rangle_{\mathrm{HS}} - \langle \mathbf{S}^2 \rangle_{\mathrm{BS}})} \quad (3)$$

Here, E_{BS} and E_{HS} represent the energy of the broken symmetry solution and the high-spin state, respectively, and $\langle \mathbf{S}^2 \rangle_{\mathrm{HS}}$ and $\langle \mathbf{S}^2 \rangle_{\mathrm{BS}}$ stand for the $\langle \mathbf{S}^2 \rangle$ values of the two states. Other procedures to estimate the energy difference include more lengthy prescriptions discussed by Kitagawa et al.,[66] Malrieu and Trinquier,[67] Saito and Thiel,[68] and Chu et al.[69] and have been applied to somewhat smaller diradicals. Keeping in mind the computational cost of the large systems under study, we have used eq 3 to calculate the coupling constants for diradicals.

To determine the intersite coupling constants in polyradicals, the Heisenberg−Dirac−van Vleck (HDvV) Hamiltonian can be used. The HDvV Hamiltonian is written as

$$H_{\mathrm{HD_vV}} = -2 \sum_{(i<j)}^{\mathrm{atom}} J_{ij} S(i) \cdot S(j) \quad (4)$$

where i and j are the radical sites with local spin $S(i)$ and $S(j)$. Note that here, J_{ij} is dependent on the identities of the two sites being coupled. Generally, the HDvV Hamiltonian is used for understanding spin couplings in transition-metal complexes; however, it has also been shown to be useful in the treatment of organic polyradicals.[70,71] The coupling constants for polyradicals have been determined following the procedure of Pantazis et al.[72] The energies of BS states with distinct spin configurations were computed, and since the number of coupling constants is less than the number of states, the resulting equations were solved using singular value decomposition to obtain unique solutions for J_{ij}. Our procedure is presented in detail in Section 1 of the Supporting Information. Final energy levels were obtained from direct diagonalization of the HDvV Hamiltonian.

2.3. Computational Details. We have carried out the full, high-level optimization on the mono- and diradical test sets (vide infra, Figures 1 and 2, respectively) using B3LYP[73−75]

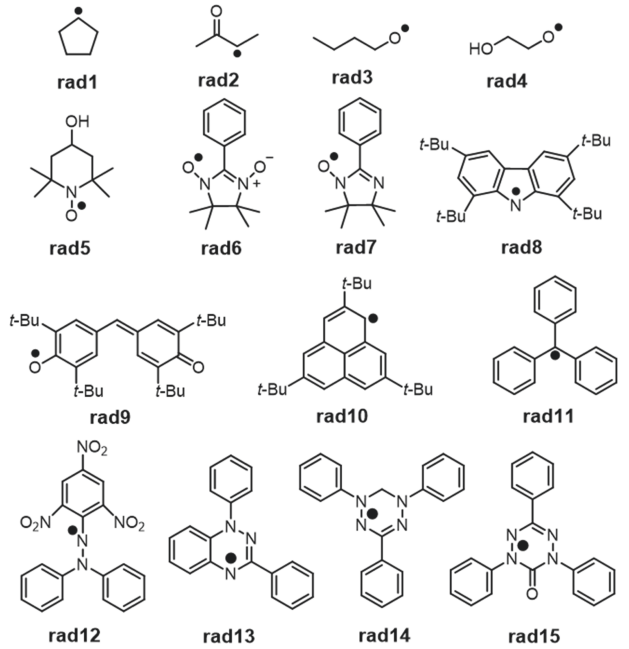

Figure 1. Structures of 15 monoradicals included in the Mono15 test set.

with Grimme's D3 dispersion correction[76] and Becke−Johnson damping[77] using the 6-311++G(d,p) basis set.[78−82] Diradicals were optimized at the high level for both the singlet and triplet states. Minimum energy structures were confirmed through frequency calculations at the B3LYP-D3BJ/6-311++G(d,p) level of theory. The corresponding total energies and properties are used as the reference values throughout all tests. All MIM2 calculations were performed with B3LYP-D3BJ/6-311++G(d,p) as the high level of theory and B3LYP-D3BJ/6-31G(d) as the low level of theory. The use of the same functional with differing basis sets helps to avoid potential mismatches between functionals while still representing a substantial increase in accuracy through the difference in basis set size. MIM2 single-point energies were obtained with dimer and trimer subsystems for each molecule in both test sets. We

DOI: 10.1021/acs.jctc.9b00563
J. Chem. Theory Comput. 2019, 15, 5998−6009

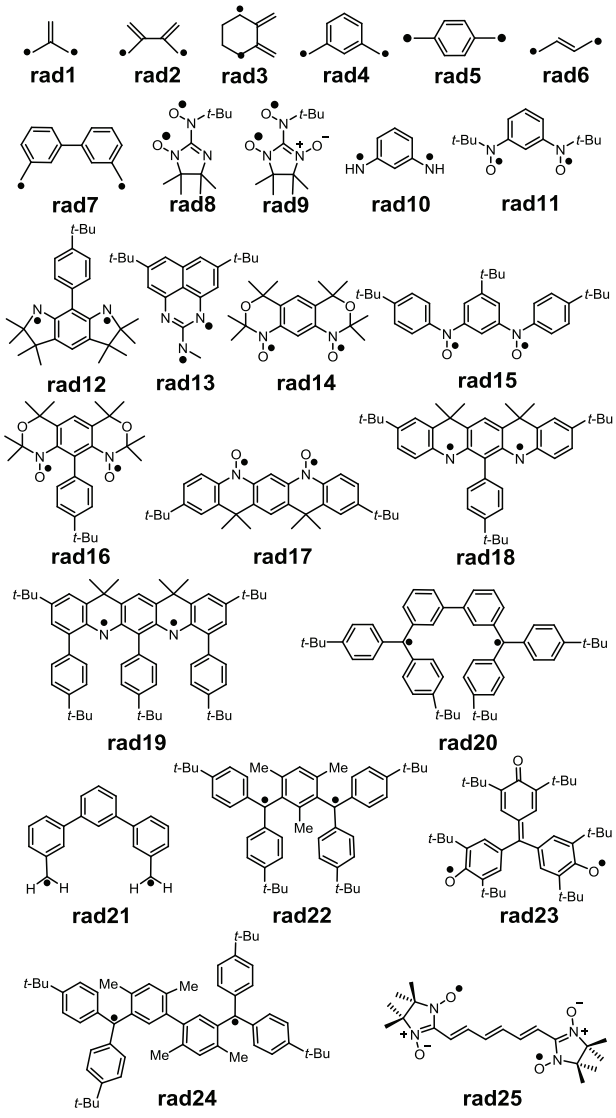

Figure 2. Structures of 25 diradicals included in the Di25 test set.

have also tested the effect of the long-range corrected functional CAM-B3LYP on the mono- and diradicals to evaluate the error in MIM2 energy by calculating the single-point energies using 6-31++G(d,p) as the high level basis set and 6-31G(d) as the low level.

To stress test MIM on larger open-shell systems with many possible spin states, we have studied the polyradicals shown in Figure 3 (vide infra). Due to the larger size of these molecules, we have adopted the B3LYP-D3BJ/6-311G(d) level of theory for full optimization in the highest spin state; further spin states were not optimized, and excitations are assumed to be vertical in nature. Next, the single-point energies of the high-spin state (HS) and broken symmetry states (BS) were evaluated at B3LYP-D3BJ/6-311++G(d,p). Finally, the deviation of the single-point energies (ΔE) between full and fragmented (using dimer, trimer, and tetramer subsystems) calculations were determined for the HS and BS states of the polyradicals. All calculations were performed in the gas phase under the framework of unrestricted density functional theory using the Gaussian (G16) program suite.[83]

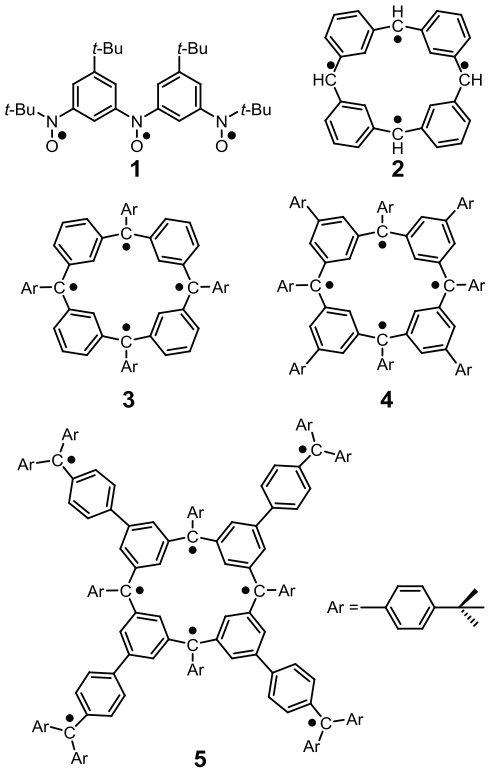

Figure 3. Structures of examined polyradicals.

3. RESULTS AND DISCUSSION

To assess the applicability of the MIM fragmentation method to open-shell molecules of disparate spin states, a careful benchmark study is performed on organic radicals. First, we test MIM on a set of 15 small- to medium-sized monoradical species (the Mono15 test set), as shown in Figure 1. Next, to determine the ability of MIM to reproduce radical coupling effects, we evaluate MIM on the triplet state of 25 diradicals (the Di25 test set), as depicted in Figure 2, as well as the open-shell singlet state (i.e., broken symmetry, BS state) of the 22 applicable molecules in the Di25 set. Finally, to assess the performance of MIM on systems with a larger number of radical centers, we have also studied the tri-, tetra-, and octaradicals depicted in Figure 3. The molecules are fragmented following the fragmentation schemes described in Section 2.3 and the Supporting Information (Figures S2−S4). Results presented throughout this section are calculated using the B3LYP-D3BJ method unless otherwise mentioned explicitly.

We have not yet implemented the evaluation of the total $\langle \mathbf{S}^2 \rangle$ value from the fragment calculations. Therefore, in the calculation of coupling constants, we have considered the $\langle \mathbf{S}^2 \rangle$ value derived from the low-level calculation on the full molecule ($E^{\mathrm{R}}_{\mathrm{low}}$ in eq 1). To determine if this is an appropriate approximation, Figure 4 details the mean deviation in $\langle \mathbf{S}^2 \rangle$ at both the low and high levels of theory from the directly evaluated $\langle \mathbf{S}^2 \rangle$ values for the monoradical set and both spin states of the diradical set. We refer to the deviation of the calculated $\langle \mathbf{S}^2 \rangle$ from the ideal value as $\Delta\langle \mathbf{S}^2 \rangle$. For the doublet state of the monoradicals, there is almost no difference between the low- and high-level mean $\Delta\langle \mathbf{S}^2 \rangle$ value. In the case of diradicals, the difference between low and high levels is again quite small: 0.003 for triplet states and 0.004 for broken symmetry singlets. Thus, the low level $\langle \mathbf{S}^2 \rangle$ value seems

DOI: 10.1021/acs.jctc.9b00563
J. Chem. Theory Comput. 2019, 15, 5998−6009

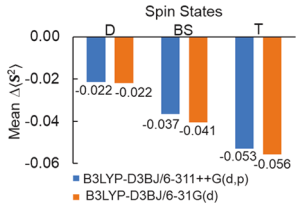

Figure 4. Mean $\Delta\langle S^2\rangle$ with respect to ideal value of the Mono15 and Di25 benchmark sets. D, BS, and T represent doublet, broken symmetry singlet, and triplet states, respectively.

appropriate for the calculation of coupling constants and comparison to experiments.

3.1. Monoradicals. The 15 monoradicals shown in Figure 1 are experimentally known and exhibit doublet ground states.[84,85] These radicals contain diverse functional groups, disparate hybridizations, and radical centers at differing p-block elements. In addition, some of the molecules included in the Mono15 test set contain cyclic, conjugated moieties stabilizing the radical center. The $\langle S^2\rangle$ values and energies of all studied radicals are provided in the Supporting Information, Table S2. The error in the calculation of the energy (ΔE), with respect to the full calculation, for each radical of the Mono15 test set is shown in Figure 5. In this test set, every subsystem in the MIM scheme is either a doublet (if it contains the radical center) or closed-shell singlet (otherwise).

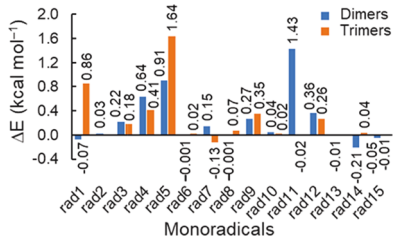

Figure 5. Errors in the energy (ΔE) of MIM2[B3LYP-D3BJ/6-311++G(d,p):B3LYP-D3BJ/6-31G(d)] using dimer and trimer subsystems with respect to the full, high level calculation, on the Mono15 set.

While the results of MIM2 with the dimer model are in very good agreement (<1 kcal mol^{-1} in all but one case, rad11) with the full calculation, we have also included the results of MIM2 using the trimer model, wherever applicable (Figure 5, rad2, and rad13 do not have more than three primitive monomers and are omitted). All errors are less than 2 kcal mol^{-1}, ranging from 0.001 to 1.43 kcal mol^{-1} for the dimer model and 0.01 to 1.64 kcal mol^{-1} for the trimer model (Figure 5). The largest dimer error, rad11 with 1.43 kcal mol^{-1}, arises from the triphenylmethyl radical, which is expected as every dimer primary subsystem includes the radical center and only one phenyl group, meaning a tertiary radical is now represented as a primary radical. Upon expansion to the trimer scheme, every primary subsystem in rad11 contains two phenyl groups and the secondary radical center, indicating that the radical delocalization is better described in trimer subsystems containing two phenyl rings compared to the dimer with only one phenyl ring to significantly reduce the error (to 0.02 kcal mol^{-1}).

In most of the cases shown in Figure 5, the error is substantially reduced when considering a trimer scheme as opposed to a dimer scheme, with two notable exceptions. Both rad1 and rad5 perform significantly worse as trimers than as dimers and are also the only cases where rings are broken during fragmentation. This result likely stems from repulsion between the two link atoms in each primary trimer subsystem, making the less-strained dimer subsystems more appropriate and hence more reliable. Additionally, we also observed that the repulsion between those link atoms is treated differently by the high and low levels of theory, resulting in an overall larger error. The mean absolute error (MAE) in B3LYP-D3BJ calculated energy is very similar using both models (0.27 kcal mol^{-1} for the dimer model and 0.31 kcal mol^{-1} for the trimer model); however, the trimer scheme outperforms the dimer scheme significantly when considering larger systems (vide infra). If the contribution from those two structures is not included, we indeed see a decrease in MIM2 errors going from dimer to trimer subsystems (dimers MAE: 0.26 kcal/mol; trimers MAE: 0.14 kcal/mol). However, it is important to note that the overall errors are quite small for both dimer and trimer subsystems. Similar accuracy was observed with CAM-B3LYP (MAE = 0.35 kcal mol^{-1}), as shown in Table S3. This first test confirms that in the case of monoradicals, MIM performs as well as it does for closed-shell systems. The only considerations that must be made to ensure accuracy are avoidance of ring-breaking and ensuring tertiary radicals are at least represented as secondary radicals in individual subsystems.

3.2. Diradicals. To determine the best procedure for the fragmentation of systems with a diradical character, we first study the triplet states of the 25 diradicals present in the Di25 test set, as shown in Figure 2. These 25 radicals are experimentally known, have different sizes and hybridizations with radical centers at different p-block elements, such as C, N, and O, and some of them contain cyclic, conjugated moieties. The $\langle S^2\rangle$ values and energies of the full radicals are provided in the Supporting Information, Table S4. The MIM2 results are compared to the full calculations at B3LYP-D3BJ/6-311++G(d,p) and detailed in Table 1. In this comparison, for the triplet spin state, each MIM subsystem is either in a doublet, triplet, or a closed-shell singlet state depending on the presence of one, two, or no radical centers, respectively. The MIM error ranges from 0.03 to 4.97 kcal mol^{-1} for the dimer model and 0.001 to 1.43 kcal mol^{-1} for the trimer model (Table 1). The MAE in energy is 0.80 kcal mol^{-1} for the dimer model and 0.38 kcal mol^{-1} for the trimer model, showcasing general improvement in the trimer model. As a test, we have calculated the MIM error obtained for the triplet state for the trimer model employing CAM-B3LYP functional and it follows the same trend as that obtained with B3LYP-D3BJ (Table S5).

In addition to the triplet states, we report the performance of MIM on the open-shell singlet states of the 22 applicable diradicals in the Di25 test set. The broken symmetry state of rad1 is too conjugated for the proper application of MIM, and the lower spin state of rad5 and rad6 are closed-shell singlets, which is outside the scope of this work. Similar to the triplet states, we compared the MIM2 results with the full calculation at B3LYP-D3BJ/6-311++G(d,p) and employed dimer and trimer models wherever applicable. For broken symmetry solutions of diradicals in the MIM calculation, each subsystem is either a doublet, open-shell singlet, or a closed-shell singlet, depending on the presence of one, two, or no radical centers, respectively. The $\langle S^2\rangle$ values and energies of the full radicals are provided in the Supporting Information, Table S6. The MIM error in energy ranges from 0.01 to 4.97 kcal mol^{-1} for the dimer model and 0.003 to 1.50 kcal mol^{-1} for the trimer model with MAEs of 0.84 and 0.48 kcal mol^{-1}, respectively.

DOI: 10.1021/acs.jctc.9b00563
J. Chem. Theory Comput. 2019, 15, 5998−6009

Table 1. Performance of MIM on Di25 Benchmark Set[a]

	ΔE_T		ΔE_S		J^Y		ΔE_{ST}		
	Dimers	Trimers	Dimers	Trimers	Full	MIM	Full	MIM	Literature
rad1	0.21	NA	-	-	-	-	-	-	
rad2	0.32	0.05	0.29	0.01	−0.84	−0.84	−1.68	−1.68	
rad3	0.2	−0.45	0.30	−0.41	−1.97	−2.04	−3.94	−4.08	
rad4	0.11	NA	−0.20	NA	6.09	6.35[b]	12.17	12.70[b]	~ 10 [85]
rad5	0.003	NA	-	-	-	-	-	-	
rad6	−0.32	NA	-	-	-	-	-	-	
rad7	−0.02	−0.02	0.01	−0.003	−0.28	−0.30	−0.56	−0.60	
rad8	0.48	0.21	0.13	−0.16	1.32	1.67	2.64	3.35	2.2 [17]
rad9	0.98	0.23	−0.45	−1.19	1.57	2.95	3.14	5.89	1.6 [17]
rad10	0.14	NA	−0.20	NA	6.87	7.19[b]	13.73	14.37[b]	
rad11	0.004	−0.09	0.31	0.05	0.96	0.82	1.92	1.64	≥ RT ≈ 0.6 (SQUID) [86] ~ 1.8 (BS-DFT) [84] ≈ 1.6 (DDCI) [87]
rad12	0.50	−0.82	−0.14	−1.50	5.43	6.10	10.87	12.19	11.0 (BS-DFT)[88] 9.6 (Barone's DDCI)[89]
rad13	0.10	−0.001	−0.35	−0.46	4.84	5.26	9.68	10.53	8-10 (UB3LYP/6-31G* and CASPT2/6-31G*).[90]
rad14	−0.48	−0.22	−0.50	−0.25	1.30	1.33	2.60	2.66	≥ RT ≈ 0.6 (SQUID) ~ 3.3 (BS-DFT) [20]
rad15	−0.13	0.25	−0.23	0.20	0.67	0.72	1.34	1.44	~ 1.5 – 1.8 (BS-DFT)[91]
rad16	−0.40	0.59	−0.46	0.54	0.94	0.99	1.89	1.98	≈ 0.8 – 1.6 (SQUID) 2.2 (BS-DFT) [20]
rad17	−0.11	−0.11	−0.15	−0.15	0.78	0.82	1.57	1.65	≥ 0.6 (SQUID), [19] ~ 2.0 (BS-DFT), [92] ~ 0.6 (DDCI) [93]
rad18	0.10	−0.20	−0.20	−0.51	3.48	3.76	6.96	7.52	~0.4 (magnetic susceptibility)[94]
rad19	1.38	0.91	1.08	0.59	3.32	3.61	6.64	7.23	~ 7.0 (BS-DFT) ~ 5.5 (DDCI)[90]
rad20	4.28	1.17	4.29	1.17	−0.08	−0.09	−0.16	−0.17	≈ −0.1[95]
rad21	−0.03	−0.04	−0.06	−0.07	0.23	0.26	0.46	0.51	
rad22	3.23	0.06	3.19	0.04	−0.03	−0.01	−0.06	−0.02	
rad23	1.14	0.67	−0.60	−0.70	4.13	5.37	8.26	10.75	
rad24	4.97	1.43	4.97	1.42	−0.03	−0.03	−0.05	−0.05	≈ 0.04 [96]
rad25	0.20	0.03	0.29	0.12	−1.48	−1.56	−2.96	−3.13	−0.19 for 1,6 dimethyl derivatives[97]
MAE	0.79	0.38	0.84	0.48		0.26		0.52	

[a]MAEs, ΔE_T, ΔE_s compared to the full, high level calculation, in kcal mol^{-1}. J^Y and ΔE_{ST} calculated as described in Methods and eq 5. N/A refers to cases where trimer calculations were not applicable. J^Y and ΔE_{ST} calculated with trimer subsystems, dimers in the nonapplicable cases. Darker shades of blue and green, referring to ΔE_s and ΔE_T, respectively, correspond to cases where improvement is seen going from dimer to trimer subsystems. The J^Ys and singlet−triplet energy gaps are shown in yellow and red shades, respectively. ΔE_{ST} with a large (>2 kcal mol^{-1}) deviation from experimental results is shown in darker red shade. [b]For dimer subsystems, the trimer scheme is not applicable.

The MAE in energy for the BS singlet states is comparable to the MAE in triplet states, suggesting that MIM is equally applicable for both spin states.

For both spin states, the errors are generally improved in the trimer model, as expected, particularly for rad20, rad22, and rad24, where ΔE is larger than 3 kcal mol^{-1} for the dimer model and improves to less than 1.5 kcal mol^{-1} when considering the trimer scheme. In the case of rad22, considering that trimer subsystems allow the spin−spin coupling interaction to be included at the high level, the error reduces to less than 0.1 kcal mol^{-1}. Considering trimer subsystems for rad20 and rad24 reduces the error similar to the behavior of the triphenylmethyl radical in the previous section: triphenyl-substituted tertiary radicals require subsystems of at least two phenyl rings to stabilize the radical and to obtain reliable results. The $|\Delta E|$ is less than 1 kcal mol^{-1} in most of the radicals investigated; however, in the case of the trimer scheme of the rad9 and rad12 BS singlet states, $|\Delta E|$ is larger than 1 kcal mol^{-1}.

In the case of rad9, the singlet state performs worse than the similar rad8, whereas the triplet state errors are nearly identical. This discrepancy raises an interesting case study exhibiting some of the complications that can occur when fragmenting diradicals. In both rad8 and rad9, the radical located on the central ring is delocalized over the oxygen and nitrogen atoms while polarizing the spin on the carbon bridging the two radical sites. In the triplet case, if the ring radical site is of α character, then the carbon is accordingly polarized to β character and acts as a buffer against the α spin radical site residing outside of the ring. However, in the broken symmetry singlet case, this spin polarization on the bridging carbon will be of the same sign as the radical located outside of the ring, meaning that cutting the carbon nitrogen bond between the two radical sites will interrupt the coupling between the two sites much more so than as a triplet. This effect is much more prominent in rad9, with the bridging carbon exhibiting a Mulliken spin density three times the magnitude of rad8. Thus, when possible, it is best to ensure both spin sites are located on

DOI: 10.1021/acs.jctc.9b00563
J. Chem. Theory Comput. 2019, 15, 5998−6009

the same monomer; however, when this is not possible, a preliminary, low level, spin density analysis can be illuminating.

Next, we have predicted the magnetic exchange coupling constant (J^Y) for each diradical with MIM and compared to the high level. As the trimer model provides a more accurate depiction of the radical environment, all coupling constants are computed using a trimer scheme. We note that for all diradicals, the calculated J^Y values correspond to an "adiabatic" coupling constant and can be seen in Table 1. In every case, MIM J^Y has the same sign as the high level coupling constant, demonstrating that the nature of coupling (ferromagnetic or antiferromagnetic) is preserved. The calculated values are in good agreement with modest deviations for rad9, rad12, and rad23, which is expected given the poorer reproduction of the BS singlet and triplet state energies observed for these species. In most of the examined diradicals, MIM overestimates the J^Y values; however, the total MAE of ΔJ^Y is quite low, 0.26 kcal mol^{-1}. We have also calculated the "vertical" coupling constant (Table S5) using the CAM-B3LYP functional, for comparison. These J values obtained from the full calculation result show that the same trend in values as that obtained from B3LYP-D3BJ with few deviations where ΔJ (B3LYP-D3BJ vs CAM-B3LYP) > 2 kcal mol^{-1} (rad10, rad12, and rad25). These deviations likely stem from the geometries being obtained with B3LYP-D3BJ, not CAM-B3LYP. Since the MIM2 error in energy for the triplet state of Di25 at CAM-B3LYP shows a similar trend to that of B3LYP-D3BJ (Table S5), the coupling constants are expected to follow the same trend for MIM2 as well.

The energy gap between the high-spin (S_{max}) and next highest-spin ($S_{max} - 1$) states can be determined from the calculated coupling constants.

$$\Delta E_{ST} = 2J^Y S_{max} \quad (5)$$

The high level and MIM calculated singlet−triplet energy gaps (ΔE_{ST}) for all applicable species are shown in Table 1. The average MIM error is nearly half a kcal mol^{-1} (MAE = 0.52 kcal mol^{-1}). A larger than 1.0 kcal mol^{-1} deviation is observed in rad9, rad12, rad13, and rad23, likely due to the poorer performance of the trimer scheme in the open-shell singlet geometry compared with the triplet state. In rad23, although both the triplet and singlet energy errors are below 1 kcal mol^{-1}, they possess opposite signs and lead to an error in J of 1.24 kcal mol^{-1}. Experimental values of ΔE_{ST} obtained from magnetic susceptibility and superconducting quantum interference device (SQUID) measurements and theoretical values of ΔE_{ST} obtained from difference-dedicated configuration interaction (DDCI) and BS-DFT are also included in Table 1. For most of the diradicals studied in this study, the calculated values are in the range of the observed values present in the literature except for rad9 and rad18. For these two radicals, even the full, high level calculation deviates significantly from the experimental ΔE_{ST} values obtained from magnetic susceptibility measurements.[17,94] Since the purpose of this study is to examine how MIM reproduces full, high level, computations, we do not expect improvement when the full calculation is itself not validated by experimental results. However, the agreement between experiment and theory in cases such as rad16 and rad17, where experimental results are matched well with both the full and MIM levels of theory and the relative trends are preserved throughout, adds validity to the levels of theory chosen for this study.

3.3. Polyradicals. To test whether MIM performs well on large, complex polyradical systems, we investigated the five polyradical systems shown in Figure 3. The first radical, **1**, the smallest among the five examined radicals, is a nitroxide-based triradical, known to have a ground state with $S = 3/2$ and a small energy gap between the quartet and lowest doublet excited state.[86−97] Three of the remaining systems are tetraradicals: **2**, **3**, and **4**, related to each other by the substitution of aromatic groups. Tetraradical **3** has been shown to exhibit an $S = 2$ ground state along with excited states of $S = 1$ and 0, the energy gap between the HS and LS states being greater than thermal energy,[98] whereas **2** and **4** were studied as related model systems in this work. The last considered polyradical is an octaradical, **5**, known as an "organic spin cluster" in the literature with $S = 4$ for the 8 ferromagnetically coupled, unpaired electrons.[99] We have studied the high-spin state for each polyradical in Figure 3 as well as several possible low m_s, broken symmetry states (Figure 6). Octaradical **5** can

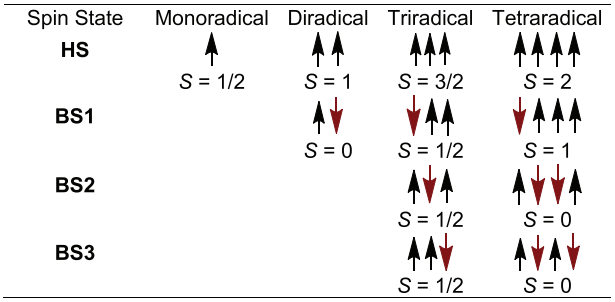

Figure 6. Spin state configurations of mono-, di-, tri-, and tetraradicals.

also be considered as a higher homologue of tetraradical **3** with an $S = 2$ macrocyclic core (tetraradical **3**) in conjunction with four biphenyl-based radical branches. The spin coupling through the macrocyclic core moiety is much stronger than the coupling between the radicals at the ends of the four branches.[99] Hence, we have studied the broken symmetry states originating from different spin combinations of the macrocyclic core, similar to that of the investigated tetraradicals. The $\langle \mathbf{S}^2 \rangle$ values and energies of the full radicals at each studied spin state are provided in the Supporting Information, Table S7.

For the high-spin state of triradical **1**, individual subsystems for the dimers are either doublets or closed-shell singlets, whereas for trimers, subsystems can be doublets, triplets, or closed-shell singlets depending on the presence of one, two, or no radical centers, respectively. In the broken symmetry states, BS1, BS2, and BS3 (Figure 7a), when $\eta = 2$, each subsystem is a doublet or a closed-shell singlet and when $\eta = 3$, subsystems are doublets, open-shell singlets, or closed-shell singlets. Due to the nonlinearity of the molecule, BS1 and BS3 have been calculated and are expected to be distinct but similar. Figure 7a shows that the error in the energy (ΔE) is greater than 1 kcal mol^{-1} in dimer subsystems but decreases to ∼0.3 kcal mol^{-1} when employing trimer subsystems with spin−spin interactions included in individual subsystems.

In the cases of tetraradicals **2**, **3**, and **4**, one HS state and three BS states exist due to molecular symmetry. The aryl groups in **3** and **4** help to stabilize the tertiary radicals and $S = 2$ in all cases with $S = 0$ and $S = 1$ comprising the lowest energy excited states. All three tetraradicals follow the stability order

DOI: 10.1021/acs.jctc.9b00563
J. Chem. Theory Comput. 2019, 15, 5998−6009

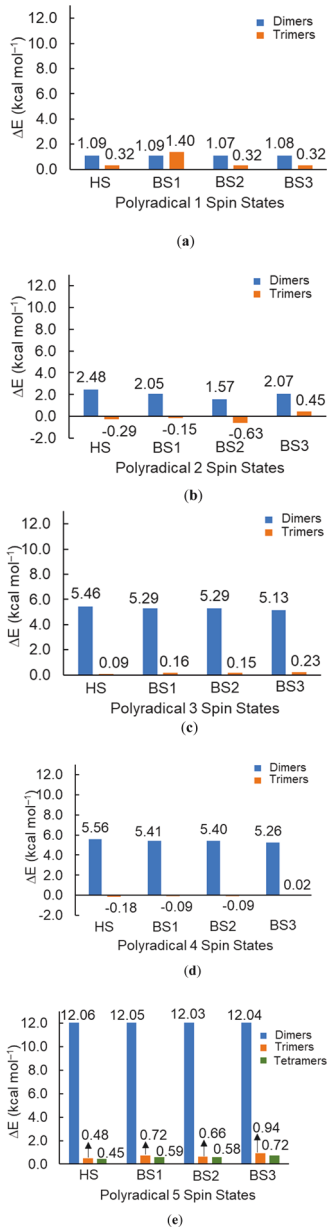

Figure 7. Energy deviation (ΔE) of MIM2[B3LYP-D3BJ/6-311++G(d,p):B3LYP-D3BJ/6-31G(d)] from the full, high level, calculation using dimer and trimer subsystems for polyradicals **1**−**5** at each applicable spin state. Tetramer subsystems were also employed for polyradical **5**, as discussed in the text.

of HS > BS2 > BS1 > BS3 (see Figure 6), although BS2 (with $S = 0$) and BS1 (with $S = 1$) are very closely spaced. In the simplest case, **2**, ΔE is greater than 2 kcal mol^{-1} with dimer subsystems, decreasing to less than 1 kcal mol^{-1} with trimer subsystems (Figure 7b). Considering the aryl substituted polyradicals **3** and **4**, ΔE is larger than 5 kcal mol^{-1} when treated with dimer subsystems. Due to increased delocalization in spin centers (Figure S5), spin−spin interactions play a very important role, increasing the errors from those obtained for tetraradical **2**. For both tetraradicals **3** and **4**, the errors decrease to below 0.2 kcal mol^{-1} when considering trimer subsystems (Figure 7c,d), indicating the applicability of this scheme even for larger systems.

To study octaradical **5**, we have considered dimer, trimer, and tetramer subsystems, improving the MIM energy systematically. The tetramer subsystems were employed to capture the spin−spin interactions not only between the central macrocyclic spin centers but also to include the interaction between the macrocyclic moiety and that of the branches. The high-spin state with $S = 4$ is the ground state, the stability order being HS > BS1 ($S = 3$) > BS3 ($S = 2$) > BS2 ($S = 2$). The energy difference between BS1 and BS3 is only 0.3 kcal mol^{-1}. The spin states of the fragmented systems are also similar to those of triradical **1** in both HS and BS states. The MIM error with dimer subsystems is greater than 12 kcal mol^{-1}, whereas with trimer and tetramer subsystems, the error reduces to below 1 kcal mol^{-1} (Figure 7e) The difference in error between trimers and tetramers is quite small, signifying that the spin coupling is very weak between the macrocyclic moiety and the branches. Hence, it can be concluded that the energy of similar polyradicals can be effectively evaluated by fragmenting it into smaller radical systems to take care of the most relevant spin−spin interactions.

Next, we have focused on the magnetic exchange coupling constants for the polyradicals using MIM2 and compared with the full high-level results. The exact wave functions that are eigenfunctions of $\mathbf{S}^2$ of different spin states are multiconfigurational and cannot be calculated within the DFT framework. Hence, we adopt the broken symmetry strategy applied for three-iron clusters by Noodleman et al.[100] The attainment of the desired BS state is confirmed from the spin density plots, as shown in Figure 8. The approximate models applied for the calculation of coupling constants are depicted in Figure 9 and

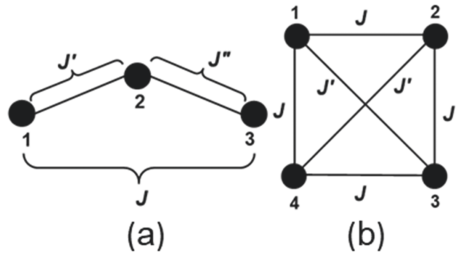

Figure 9. Approximate models applied for calculating intersite coupling constants of the (a) triradical and (b) tetraradicals.

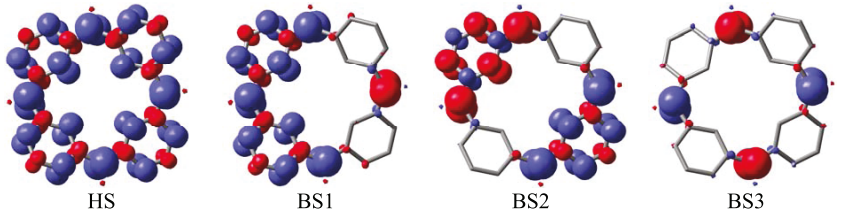

Figure 8. Spin density plots of high-spin (HS) and different broken symmetry (BS) states of polyradical **2**. The isovalue of density is 0.005 units.

DOI: 10.1021/acs.jctc.9b00563
J. Chem. Theory Comput. 2019, 15, 5998−6009

they are determined as shown in the Supporting Information, Section 1.[101,102] The resulting J's can be used to form the parametrized spin Hamiltonian and the estimates of the pure spin states are carried out by diagonalization of the Hamiltonian. As in the previous cases, in the case of polyradicals **1**−**4**, the error in energy with trimer subsystems is lower than with dimers in all spin states, except for BS1 of polyradical **1**; hence, we have used the trimer results for estimation of coupling constants. For polyradical **5**, results obtained with tetramer subsystems are used. Results along with the values corresponding to vertical coupling constants are shown in Table 2. The individual nature of coupling

Table 2. Calculated Vertical Coupling Constants of the Studied Polyradicals[a]

	J		J'		J''		
	full-high	MIM2	full-high	MIM2	full-high	MIM2	ΔE_0
1	−0.004	−0.54	0.43	−0.10	0.48	1.02	0.59
2	3.20	3.28	−0.16	−0.60			−0.04
3	1.39	1.35	−0.07	−0.07			0.16
4	1.45	1.40	−0.08	−0.07			−0.09
5	0.23	0.16	0.30	0.30			0.59

[a] J and J' are defined in Figure 9. The detailed calculation of J and J' is presented in the Supporting Information. All values are in kcal mol^{-1}.

(ferromagnetic or antiferromagnetic) matches between full high level and MIM calculations, except for J' of **1**. The MAE in ΔJ and $\Delta J'$ between full and MIM calculations is 0.06 and 0.11 kcal mol^{-1}, respectively, for polyradical **2** to **5**. The $|\Delta E|$ in BS2 of polyradical **2** (Figure 7b) is larger than for other spin states, leading to a larger deviation in J' of **2** between full and MIM calculations. In the majority of cases, the calculated coupling constant from MIM is in excellent agreement (less than 0.1 kcal mol^{-1} in 7 out of the 11 total coupling constants) with that of the full high-level calculation.

Next, we have compared the available experimental findings of the polyradical with our calculated ones. For polyradical **1**, the energy gap between quartet and lowest excited doublet state is $\Delta E_{DQ} \approx 0.5$ kcal mol^{-1}.[86] This energy gap was calculated assuming isotropic exchange interaction and neglecting the intramolecular coupling between the terminal radicals, so the spin Hamiltonian takes the form of $-2J(S_1S_2 + S_2S_3)$ and the eigenvalues of this Hamiltonian are $E_1 = 2J$ ($S = 1/2$), $E_2 = 0$ ($S = 1/2$) and $E_3 = -J$ ($S = 3/2$). For polyradical **1**, the calculated $\Delta E_{DQ} = 0.45$ kcal mol^{-1} at the high level and $\Delta E_{DQ} = 1.02$ kcal mol^{-1} with MIM2 using trimer subsystems obtained from diagonalizing the Hamiltonian, as represented in Table S8. The high-level calculation is in very good agreement with the experimental value of $\Delta E_{DQ} \approx 0.5$ kcal mol^{-1}.[86] It is clear from Table S8 that the energy levels corresponding to various spin states are very closely spaced in polyradical **1**. The larger error in BS1 resulted in a different ordering of the spin states of **1** when considering MIM2 results. In the case of polyradicals **2**−**4**, the order of stability is $S_{max} > S_{max} - 2 > S_{max} - 1 > S_{max} - 1 > S_{max} - 2$. It is clear from Table 2 that in the ground state of polyradicals **2** to **5**, the radical centers are ferromagnetically coupled and the overall magnetic interactions decrease with the increase of radical branches and the increase in aryl substitution decreases the energy gap between the different spin states. For tetraradical **3**, the most stable ground state corresponds to $S = 2$ with the lowest energy gap ∼2.5 kcal mol^{-1}. This result agrees well with the electron paramagnetic resonance spectroscopic study that has shown that tetraradical **3** possesses an $S = 2$ ground state and that the energy gap between high-spin and low-spin states is much greater than thermal energy.[98] For polyradical **5**, we have not considered the coupling between the macrocyclic core and the radical centers on the branches as these centers are far away enough to be considered noninteracting and would lead to considering unnecessary states, thus muddying the analysis. The calculated order of stability is $S_{max} > S_{max} - 1 > S_{max} - 1 > S_{max} - 2 > S_{max} - 2$. The detailed calculation is shown in Supporting Information Section 1. The ΔE between the energy levels of spin pure states calculated from full and MIM calculations is less than 1 kcal mol^{-1} for all excited states of polyradical **5**.

4. CONCLUSIONS

In this study, we have applied our multilayer Molecules-in-Molecules (MIM) fragmentation-based method to the calculation of the total energies, energy gaps, and coupling constants of open-shell organic molecules within the framework of the BS-DFT methodology. We have calibrated the performance of the MIM method using B3LYP-D3BJ and CAM-B3LYP with the 6-311++G(d,p) basis set as the high level and the 6-31G(d) basis set as the low level. The $\langle \mathbf{S}^2 \rangle$ value obtained from the low-level calculation was used for the calculation of the magnetic exchange coupling constant (J) for diradicals. For polyradicals, the intersite coupling constant has been evaluated from relevant broken symmetry state calculations. Finally, the energy of the spin pure states for large polyradicals has been calculated by diagonalizing the parametrized Hamiltonian. The energy difference between the spin pure states obtained from full and MIM2 calculations is less 1 kcal mol^{-1} in the majority of cases and in excellent agreement with experimental findings. These analyses suggest that the MIM fragmentation method can be used to study large polyradicals with several radical centers not only to obtain absolute energies but coupling constants and energy gaps as well.

■ ASSOCIATED CONTENT

Supporting Information

The Supporting Information is available free of charge on the ACS Publications website at DOI: 10.1021/acs.jctc.9b00563.

An illustrative diradical fragmentation diagram, fragmentation schemes of each molecule in each test set, equations for calculating intersite coupling constants of polyradicals, energies of full, high-level calculations (E_{high}), MIM2 with dimer subsystem ($E_{MIM2\text{-}dimers}$), MIM2 with trimer subsystem ($E_{MIM2\text{-}trimers}$), full, low-level calculations (E_{low}) in a.u. and $\langle \mathbf{S}^2 \rangle$ of full, high-level calculations ($\langle \mathbf{S}^2 \rangle_{high}$) with full, low-level calculation ($\langle \mathbf{S}^2 \rangle_{low}$) for the broken symmetry states, the calculation of coupling constants for polyradicals, and the optimized coordinates of the high spin states of all molecules (PDF)

■ AUTHOR INFORMATION

Corresponding Author

*E-mail: kraghava@indiana.edu.

ORCID

Daniel Beckett: 0000-0003-4833-2269

Bishnu Thapa: 0000-0003-3521-1062

DOI: 10.1021/acs.jctc.9b00563
J. Chem. Theory Comput. 2019, 15, 5998−6009

Krishnan Raghavachari: 0000-0003-3275-1426

Notes

The authors declare no competing financial interest.

■ ACKNOWLEDGMENTS

We acknowledge support from the National Science Foundation grant CHE-1665427 at Indiana University. T.S. was financially supported by Science and Engineering Research Board (SERB) and Indo-US Science and Technology Forum (IUSSTF) [SERB Indo-U.S. Postdoctoral Fellowship 2017/127]. D.B. was supported by the IU Presidential Diversity Dissertation Fellowship. We acknowledge the supercomputing facility at Indiana University for the computer time.

■ REFERENCES

(1) *Reactive Intermediate Chemistry*; Moss, R. A.; Platz, M. S.; Jones, M., Jr., Eds.; Wiley-Interscience: New York, 2004.
(2) Rajca, A.; Wongsriratanakul, J.; Rajca, S. High-spin organic polyradicals as spin clusters: ferromagnetic spin coupling through biphenyl unit in polyarylmethyl tri-, penta-, hepta-, and hexadecarradicals. *J. Am. Chem. Soc.* **1997**, *119*, 11674−11686.
(3) Bourissou, D.; Guerret, O.; Gabbaï, F.; Bertrand, G. Stable carbenes. *Chem. Rev.* **2000**, *100*, 39−91.
(4) Hopkinson, M.; Richter, C.; Schedler, M.; Glorius, F. An overview of N-heterocyclic carbenes. *Nature* **2014**, *510*, 485−496.
(5) Rajca, A.; Wongsriratanakul, J.; Rajca, S. Magnetic ordering in an organic polymer. *Science* **2001**, *294*, 1503−1505.
(6) Rajca, A. The physical organic chemistry of very high-spin polyradicals. *Adv. Phys. Org. Chem.* **2005**, *40*, 153−199.
(7) Wingate, A. J.; Boudouris, B. W. J. Recent advances in the syntheses of radical-containing macromolecules. *Polym. Sci., Part A: Polym. Chem.* **2016**, *54*, 1875−1894.
(8) Sanvito, S. Molecular spintronics. *Chem. Soc. Rev.* **2011**, *40*, 3336−3355.
(9) Shil, S.; Bhattacharya, D.; Misra, A.; Klein, D. J. A high-spin organic diradical as a spin filter. *Phys. Chem. Chem. Phys.* **2015**, *17*, 23378−23383.
(10) Tsuji, Y.; Hoffmann, R.; Strange, M.; Solomon, G. C. Close relation between quantum interference in molecular conductance and diradical existence. *Proc. Natl. Acad. Sci. U.S.A.* **2016**, *113*, E413−E419.
(11) Gaudenzi, R.; Burzuri, E.; Reta, D.; Moreira, I. deP. R.; Bromley, S. T.; Rovira, C.; Veciana, J.; van der Zant, H. S. J. Exchange coupling inversion in a high-spin organic triradical molecule. *Nano Lett.* **2016**, *16*, 2066−2071.
(12) Herrmann, C.; Solomon, G. C.; Ratner, M. A. Organic radicals as spin filters. *J. Am. Chem. Soc.* **2010**, *132*, 3682−3684.
(13) Jahn, B. O.; Ottosson, H.; Galperin, M.; Fransson, J. Organic single molecular structures for light induced spin-pump devices. *ACS Nano* **2013**, *7*, 1064−1071.
(14) Abe, M. Diradicals. *Chem. Rev.* **2013**, *113*, 7011−7088.
(15) Miller, J. S. Magnetically ordered molecule-based assemblies. *Dalton Trans.* **2006**, 2742−2749.
(16) Hiraoka, S.; Okamoto, T.; Kozaki, M.; Shiomi, D.; Sato, K.; Takui, T.; Okada, K. A stable radical-substituted radical cation with strongly ferromagnetic interaction: nitronyl nitroxide-substituted 5,10-diphenyl-5,10-dihydrophenazine radical cation. *J. Am. Chem. Soc.* **2004**, *126*, 58−59.
(17) Suzuki, S.; Furui, T.; Kuratsu, M.; Kozaki, M.; Shiomi, D.; Sato, K.; Takui, T.; Okada, K. Nitroxide-substituted nitronyl nitroxide and iminonitroxide. *J. Am. Chem. Soc.* **2010**, *132*, 15908−15910.
(18) Inoue, K.; Iwamura, H. 2-[p(n-tert-butyl-n-oxyamino)phenyl]-4,4,5,5-tetramethyl-4,5-dihydroimidazol-3-oxide-1-oxyl, a stable diradical with a triplet ground state. *Angew. Chem., Int. Ed.* **1995**, *34*, 927−928.
(19) Rajca, A.; Shiraishi, K.; Rajca, S. Stable diarylnitroxide diradical with triplet ground state. *Chem. Commun.* **2009**, 4372−4374.
(20) Rajca, A.; Takahashi, M.; Pink, M.; Spagnol, G.; Rajca, S. Conformationally constrained, stable, triplet ground state (s = 1) nitroxide diradicals. Antiferromagnetic chains of s = 1 diradicals. *J. Am. Chem. Soc.* **2007**, *129*, 10159−10170.
(21) Rassat, A.; Sieveking, U. A stable aromatic diradical with strong dipolar electronic interaction. *Angew. Chem., Int. Ed.* **1972**, *11*, 303−304.
(22) Boratyński, P. J.; Pink, M.; Rajca, S.; Rajca, A. Isolation of the triplet ground state aminyl diradical. *Angew. Chem., Int. Ed.* **2010**, *49*, 5459−5462.
(23) Shultz, D. A.; Fico, R. M.; Lee, H.; Kampf, J. W.; Kirschbaum, K.; Pinkerton, A. A.; Boyle, P. D. Mechanisms of exchange modulation in trimethylenemethane-type biradicals: the roles of conformation and spin density. *J. Am. Chem. Soc.* **2003**, *125*, 15426−15432.
(24) Fukuzaki, E.; Nishide, H. Room-temperature high-spin organic single molecule: nanometer-sized and hyperbranched poly[1,2,(4)-phenylenevinyleneanisylaminium]. *J. Am. Chem. Soc.* **2006**, *128*, 996−1001.
(25) Veciana, J.; Rovira, C.; Crespo, M. I.; Armet, O.; Domingo, V. M.; Palacio, F. Stable polyradicals with high-spin ground states. 1. Synthesis, separation, and magnetic characterization of the stereoisomers of 2,4,5,6-tetrachloro-.alpha.,.alpha.,.alpha.′,.alpha.′-tetrakis-(pentachlorophenyl)-m-xylylene biradical. *J. Am. Chem. Soc.* **1991**, *113*, 2552−2561.
(26) Rajca, A.; Utamapanya, S. pi.-Conjugated systems with unique electronic structure: a case of planarized 1,3-connected polyarylmethyl carbodianion and stable triplet hydrocarbon diradical. *J. Org. Chem.* **1992**, *57*, 1760−1767.
(27) Raghavachari, K.; Trucks, G. W.; Pople, J. A.; Head-Gordon, M. A fifth-order perturbation comparison of electron correlation theories. *Chem. Phys. Lett.* **1989**, *157*, 479−483.
(28) Chen, W.; Schlegel, H. B. Evaluation of S^2 for correlated wave functions and spin projection of unrestricted Mo/ller−Plesset perturbation theory. *J. Chem. Phys.* **1994**, *101*, 5957−5968.
(29) Noga, J.; Bartlett, R. J. The full CCSDT model for molecular electronic structure. *J. Chem. Phys.* **1987**, *86*, 7041−7050.
(30) Stanton, J. F. Why CCSD(T) works: a different perspective. *Chem. Phys. Lett.* **1997**, *281*, 130−134.
(31) Bartlett, R. J. Coupled-cluster approach to molecular structure and spectra: a step toward predictive quantum chemistry. *J. Phys. Chem. A* **1989**, *93*, 1697−1708.
(32) Langhoff, S. R. *Quantum Mechanical Electronic Structure Calculations with Chemical Accuracy*; Kluwer Academic Publishers: Dordrecht; Boston, 1995.
(33) Crawford, T. D.; Kraka, E.; Stanton, J. F.; Cremer, D. Problematic p-benzyne: Orbital instabilities, biradical character, and broken symmetry. *J. Chem. Phys.* **2001**, *114*, 10638−10650.
(34) Li, X. H.; Paldus, J. Reduced multireference coupled cluster method with singles and doubles: Perturbative corrections for triples. *J. Chem. Phys.* **2006**, *124*, 174101−174113.
(35) Krylov, A. I. The quantum chemistry of open-shell species. *Rev. Comput. Chem.* **2017**, *30*, 151−224.
(36) Glaesemann, K. R.; Schmidt, M. W. On the Ordering of Orbital Energies in High-Spin ROHF. *J. Phys. Chem. A* **2010**, *114*, 8772−8777.
(37) Parkinson, C. J.; Mayer, P. M.; Radom, L. An assessment of theoretical procedures for the calculation of reliable radical stabilization energies. *J. Chem. Soc., Perkin Trans. 2* **1999**, *1999*, 2305−2313.
(38) Menon, A. S.; Radom, L. Consequences of spin contamination in unrestricted calculations on open-shell species: effect of hartree−fock and møller−plesset contributions in hybrid and double-hybrid density functional theory approaches. *J. Phys. Chem. A* **2008**, *112*, 13225−13230.
(39) Menon, A. S.; Wood, G. P. F.; Moran, D.; Radom, L. Bond dissociation energies and radical stabilization energies: an assessment of contemporary theoretical procedures. *J. Phys. Chem. A* **2007**, *111*, 13638−13644.

DOI: 10.1021/acs.jctc.9b00563
J. Chem. Theory Comput. 2019, 15, 5998−6009

(40) Menon, A. S.; Radom, L. Consequences of spin contamination in unrestricted calculations on open-shell species: effect of Hartree−Fock and Møller−Plesset contributions in hybrid and double-hybrid density functional theory approaches. *J. Phys. Chem. A* **2008**, *112*, 13225−13230.
(41) Pople, J. A.; Gill, P. M. W.; Handy, N. C. Spin-unrestricted character of Kohn−Sham orbitals for open-shell systems. *Int. J. Quantum Chem.* **1995**, *56*, 303−305.
(42) Feller, D.; Davidson, E. R.; Borden, W. T. Ab initio calculations of the energy difference between trimethylenemethane and butadiene. *Isr. J. Chem.* **1983**, *23*, 105−108.
(43) Kato, S.; Morokuma, K.; Feller, D.; Davidson, E. R.; Borden, W. T. Ab initio study of m-benzoquinodimethane. *J. Am. Chem. Soc.* **1983**, *105*, 1791−1795.
(44) Raghavachari, K.; Saha, A. Accurate composite and fragment-based quantum chemical models for large molecules. *Chem. Rev.* **2015**, *115*, 5643−5677.
(45) Collins, M. A.; Bettens, R. P. A. Energy-based molecular fragmentation methods. *Chem. Rev.* **2015**, *115*, 5607−5642.
(46) Gordon, M. S.; Fedorov, D. G.; Pruitt, S. R.; Slipchenko, L. V. Fragmentation methods: A route to accurate calculations on large systems. *Chem. Rev.* **2012**, *112*, 632−672.
(47) Saha, A.; Raghavachari, K. Dimers of dimers (DOD): A new fragment-based method applied to large water clusters. *J. Chem. Theory Comput.* **2014**, *10*, 58−67.
(48) Mayhall, N. J.; Raghavachari, K. Molecules-in-Molecules: An extrapolated fragment-based approach for accurate calculations on large molecules and materials. *J. Chem. Theory Comput.* **2011**, *7*, 1336−1343.
(49) Saha, A.; Raghavachari, K. Analysis of different fragmentation strategies on a variety of large peptides: Implementation of a low level of theory in fragment-based methods can be a crucial factor. *J. Chem. Theory Comput.* **2015**, *11*, 2012−2023.
(50) Jose, K. V. J.; Raghavachari, K. Evaluation of energy gradients and infrared vibrational spectra through Molecules-in-Molecules fragment-based approach. *J. Chem. Theory Comput.* **2015**, *11*, 950−961.
(51) Jose, K. V. J.; Raghavachari, K. Fragment-based approach for the evaluation of NMR chemical shifts for large biomolecules incorporating the effects of the solvent environment. *J. Chem. Theory Comput.* **2017**, *13*, 1147−1158.
(52) Thapa, B.; Beckett, D.; Jose, K. V. J.; Raghavachari, K. Assessment of fragmentation strategies for large proteins using the multilayer molecules-in-molecules approach. *J. Chem. Theory Comput.* **2018**, *14*, 1383−1394.
(53) Thapa, B.; Beckett, D.; Erickson, J.; Raghavachari, K. Theoretical study of protein−ligand interactions using the molecules-in-molecules fragmentation-based method. *J. Chem. Theory Comput.* **2018**, *14*, 5143−5155.
(54) Li, H.; Liu, W.; Suo, B. Localization of open-shell molecular orbitals via least change from fragments to molecule. *J. Chem. Phys.* **2017**, *146*, No. 104104.
(55) Pruitt, S. R.; Fedorov, D. G.; Kitaura, K.; Gordon, M. S. Open-shell formulation of the fragment molecular orbital method. *J. Chem. Theory Comput.* **2010**, *6*, 1−5.
(56) Nakata, H.; Fedorov, D. G.; Kitaura, K.; Nakamura, S. Extension of the fragment molecular orbital method to treat large open-shell systems in solution. *Chem. Phys. Lett.* **2015**, *635*, 86−92.
(57) Chung, L. W.; Sameera, W. M.; Ramozzi, R.; Page, A. J.; Hatanaka, M.; Petrova, G. P.; Harris, T. V.; Li, X.; Ke, Z.; Liu, F.; Li, H. B.; Ding, L.; Morokuma, K. The oniom method and its applications. *Chem. Rev.* **2015**, *115*, 5678−5796.
(58) Svensson, M.; Humbel, S.; Froese, R. D. J.; Matsubara, T.; Sieber, S.; Morokuma, K. Oniom: A multilayered integrated MO + MM method for geometry optimizations and single point energy predictions. A test for Diels−Alder reactions and $Pt(P(t\text{-}bu)_3)_2 + H_2$ oxidative addition. *J. Phys. Chem. A* **1996**, *100*, 19357−19363.
(59) Borden, W. T.; Davidson, E. R.; Feller, D. RHF and two configuration SCF calculations are inappropriate for conjugated diradicals. *Tetrahedron* **1982**, *38*, 737−739.
(60) Noodleman, L. Valence bond description of antiferromagnetic coupling in transition metal dimers. *J. Chem. Phys.* **1981**, *74*, 5737−5744.
(61) Noodleman, L.; Baerends, E. J. Electronic structure, magnetic properties, ESR, and optical spectra for 2-iron ferredoxin models by LCAO-X.alpha. valence bond theory. *J. Am. Chem. Soc.* **1984**, *106*, 2316−2327.
(62) Noodleman, L.; Davidson, E. R. Ligand spin polarization and antiferromagnetic coupling in transition metal dimers. *Chem. Phys.* **1986**, *109*, 131−143.
(63) Noodleman, L.; Peng, C. Y.; Case, D. A.; Mouesca, J.-M. Orbital Interactions, Electron Delocalization and Spin Coupling In Iron-Sulfur Clusters. *Coord. Chem. Rev.* **1995**, *144*, 199−244.
(64) Yamaguchi, K.; Fukui, H.; Fueno, T. Molecular orbital (MO) theory for magnetically interacting organic compounds. Ab-initio MO Calculations of the Effective Exchange Integrals for cyclophanetype Carbene Dimers. *Chem. Lett.* **1986**, 625−628.
(65) Yamaguchi, K.; Takahara, Y.; Fueno, T.; Houk, K. N. Extended Hartree-Fock (EHF) theory of chemical reactions. *Theor. Chim. Acta* **1988**, *73*, 337−364.
(66) Kitagawa, Y.; Saito, T.; Nakanishi, Y.; Kataoka, Y.; Matsui, T.; Kawakami, T.; Okumura, M.; Yamaguchi, K. Development of approximately spin projected energy derivatives for biradical systems. *Int. J. Quantum Chem.* **2010**, *110*, 3053−3060.
(67) Malrieu, J. P.; Trinquier, G. A recipe for geometry optimization of diradicalar singlet states from broken-symmetry calculations. *J. Phys. Chem. A* **2012**, *116*, 8226−8237.
(68) Bazewicz, C. G.; Lipkin, J. S.; Smith, E. E.; et al. Expanding the Utility of 4-Cyano-L-Phenylalanine as a vibrational reporter of protein environments. *J. Phys. Chem. B* **2012**, *116*, 10824−10831.
(69) Chu, S.; Bovi, D.; Cappelluti, F.; Orellana, A. G.; Martin, H.; Guidoni, L. Effects of static correlation between spin centers in multicenter transition metal complexes. *J. Chem. Theory Comput.* **2017**, *13*, 4675−4683.
(70) Illas, F.; Moreira, I. P. R.; Graaf, C.; Barone, V. Magnetic coupling in biradicals, binuclear complexes and wide gap insulators: a survey of ab initio wave function and density functional theory approaches. *Theor. Chem. Acc.* **2000**, *104*, 265−272.
(71) Muñoz, D.; Moreira, I. P. R.; Illas, F. Effective t-J model Hamiltonian parameters of monolayered cuprate superconductors from ab initio electronic structure calculations. *Phys. Rev. B* **2002**, *65*, 224521−224536.
(72) Pantazis, D. A.; Orio, M.; Petrenko, T.; Zein, S.; Bill, E.; Lubitz, W.; Messinger, J.; Neese, F. A New quantum chemical approach to the magnetic properties of oligonuclear transition-metal complexes: application to a model for the tetranuclear manganese cluster of photosystem II. *Chem. − Eur. J.* **2009**, *15*, 5108−5123.
(73) Becke, A. D. Density-functional thermochemistry. I. The effect of the exchange-only gradient correction. *J. Chem. Phys.* **1992**, *96*, 2155−2160.
(74) Lee, C.; Yang, W.; Parr, R. G. Development of the Colle-Salvetti correlation-energy formula into a functional of the electron density. *Phys. Rev. B: Condens. Matter Mater. Phys.* **1988**, *37*, 785−789.
(75) Stephens, P.; Devlin, F.; Chabalowski, C.; Frisch, M. J. Ab initio calculation of vibrational absorption and circular dichroism spectra using density functional force fields. *J. Phys. Chem. A* **1994**, *98*, 11623−11627.
(76) Grimme, S.; Antony, J.; Ehrlich, S.; Krieg, H. A consistent and accurate ab initio parametrization of density functional dispersion correction (DFT-D) for the 94 elements H-Pu. *J. Chem. Phys.* **2010**, *132*, No. 154104.
(77) Grimme, S.; Ehrlich, S.; Goerigk, L. Effect of the damping function in dispersion corrected density functional theory. *J. Comput. Chem.* **2011**, *32*, 1456−1465.
(78) Clark, T.; Chandrasekhar, J.; Spitznagel, G. W.; Schleyer, P. V. R. Efficient diffuse function-augmented basis sets for anion

DOI: 10.1021/acs.jctc.9b00563
J. Chem. Theory Comput. 2019, 15, 5998−6009

calculations. III. The 3-21+G basis set for first-row elements, Li-F. *J. Comput. Chem.* **1983**, *4*, 294−301.
(79) Ditchfield, R.; Hehre, W. J.; Pople, J. A. Self-consistent molecular-orbital methods. IX. An extended Gaussian-type basis for molecular-orbital studies of organic molecules. *J. Chem. Phys.* **1971**, *54*, 724−728.
(80) Francl, M. M.; Pietro, W. J.; Hehre, W. J.; Binkley, J. S.; Gordon, M. S.; DeFrees, D. J.; Pople, J. A. Self-consistent molecular orbital methods. XXIII. A polarization-type basis set for second-row elements. *J. Chem. Phys.* **1982**, *77*, 3654−3665.
(81) Hariharan, P. C.; Pople, J. A. The influence of polarization functions on molecular orbital hydrogenation energies. *Theor. Chim. Acta* **1973**, *28*, 213−222.
(82) Hehre, W. J.; Ditchfield, R.; Pople, J. A. Self-consistent molecular orbital methods. XII. Further extensions of Gaussian-type basis sets for use in molecular orbital studies of organic molecules. *J. Chem. Phys.* **1972**, *56*, 2257−2261.
(83) Frisch, M. J.; Trucks, G. W.; Schlegel, H. B.; Scuseria, G. E.; Robb, M. A.; Cheeseman, J. R.; Scalmani, G.; Barone, V.; Petersson, G. A.; Nakatsuji, H.; Li, X.; Caricato, M.; Marenich, A. V.; Bloino, J.; Janesko, B. G.; Gomperts, R.; Mennucci, B.; Hratchian, H. P.; Ortiz, J. V.; Izmaylov, A. F.; Sonnenberg, J. L.; Williams-Young, D.; Ding, F.; Lipparini, F.; Egidi, F.; Goings, J.; Peng, B.; Petrone, A.; Henderson, T.; Ranasinghe, D.; Zakrzewski, V. G.; Gao, J.; Rega, N.; Zheng, G.; Liang, W.; Hada, M.; Ehara, M.; Toyota, K.; Fukuda, R.; Hasegawa, J.; Ishida, M.; Nakajima, T.; Honda, Y.; Kitao, O.; Nakai, H.; Vreven, T.; Throssell, K.; Montgomery, J. A., Jr.; Peralta, J. E.; Ogliaro, F.; Bearpark, M. J.; Heyd, J. J.; Brothers, E. N.; Kudin, K. N.; Staroverov, V. N.; Keith, T. A.; Kobayashi, R.; Normand, J.; Raghavachari, K.; Rendell, A. P.; Burant, J. C.; Iyengar, S. S.; Tomasi, J.; Cossi, M.; Millam, J. M.; Klene, M.; Adamo, C.; Cammi, R.; Ochterski, J. W.; Martin, R. L.; Morokuma, K.; Farkas, O.; Foresman, J. B.; Fox, D. J. *Gaussian 16*, revision-a03; Gaussian, Inc.: Wallingford, CT, 2016.
(84) Gallagher, N. M.; Olankitwanit, A.; Rajca, A. High-spin organic molecules. *J. Org. Chem.* **2015**, *80*, 1291−1298.
(85) Wenthold, P. G.; Kim, J. B.; Lineberger, W. C. Photoelectron spectroscopy of m-xylylene anion. *J. Am. Chem. Soc.* **1997**, *119*, 1354−1359.
(86) Ishida, T.; Iwamura, H. Bis[3-tert-butyl-5-(N-oxy-tert-butylamino)phenyl] nitroxide in a quartet ground state: a prototype for persistent high-spin poly[(oxyimino)-1,3-phenylenes]. *J. Am. Chem. Soc.* **1991**, *113*, 4238−4241.
(87) Barone, V.; Cacelli, I.; Cimino, P.; Ferretti, A.; Monti, S.; Prampolini, G. Magnetic interactions in phenyl-bridged nitroxide diradicals: conformational effects by multireference and broken symmetry dft approaches. *J. Phys. Chem. A* **2009**, *113*, 15150−15155.
(88) Rajca, A.; Olankitwanit, A.; Rajca, S. Triplet ground state derivative of aza-m-xylylene diradical with large singlet−triplet energy gap. *J. Am. Chem. Soc.* **2011**, *133*, 4750−4753.
(89) Barone, V.; Boilleau, C.; Cacelli, I.; Ferretti, A.; Monti, S.; Prampolini, G. Structure−properties relationships in triplet ground state organic diradicals: a computational study. *J. Chem. Theory Comput.* **2013**, *9*, 300−307.
(90) Quast, H.; Nudling, W.; Klemm, G.; Kirschfeld, A.; Neuhaus, P.; Sander, W.; Hrovat, D. A.; Borden, W. T. A perimidine-derived non-kekulé triplet diradical. *J. Org. Chem.* **2008**, *73*, 4956−4961.
(91) Rajca, A.; Vale, M.; Rajca, S. Diarylnitroxide Diradicals: low-temperature oxidation of diarylamines to nitroxides. *J. Am. Chem. Soc.* **2008**, *130*, 9099−9105.
(92) Rajca, A.; Shiraishi, K.; Boratyn′ski, P. J.; Pink, M.; Miyasaka, M.; Rajca, S. Oxidation of annelated diarylamines: analysis of reaction pathways to nitroxide diradical and spirocyclic products. *J. Org. Chem.* **2011**, *76*, 8447−8457.
(93) Barone, V.; Cacelli, I.; Ferretti, A.; Montic, S.; Prampolini, G. Singlet−triplet energy gap of a diarylnitroxide diradical by an accurate many-body perturbative approach. *Phys. Chem. Chem. Phys.* **2011**, *13*, 4709−4714.
(94) Rajca, A.; Shiraishi, K.; Pink, M.; Rajca, S. Triplet (S = 1) Ground State Aminyl Diradical. *J. Am. Chem. Soc.* **2007**, *129*, 7232−7233.
(95) Rajca, A.; Rajca, S. Intramolecular Antiferromagnetic vs Ferromagnetic Spin Coupling through the Biphenyl Unit. *J. Am. Chem. Soc.* **1996**, *118*, 8121−8126.
(96) Rajca, A.; Utamapanya, S.; Smithhisler, D. Near-degeneracy between the low- and high-spin states in an alternant hydrocarbon diradical: topology and geometry. *J. Org. Chem.* **1993**, *58*, 5650−5652.
(97) Stroh, C.; Ziessel, R.; Raudaschl-Sieber, G.; Kohler, F. H.; Turek, P. Intramolecular exchange interactions in non-aromatic bis-nitronyl-nitroxides. *J. Mater. Chem.* **2005**, *15*, 850−858.
(98) Rajca, A.; Rajca, S.; Desai, S. R. Macrocyclic .pi.-conjugated carbopolyanions and polyradicals based upon calix[4]arene and calix[3]arene rings. *J. Am. Chem. Soc.* **1995**, *117*, 806−816.
(99) Rajca, S.; Rajca, A.; Wongsriratanakul, J.; Butler, P.; Choi, S. Organic spin clusters. A dendritic-macrocyclic poly(arylmethyl) polyradical with very high spin of s = 10 and its derivatives: synthesis, magnetic studies, and small-angle neutron scattering. *J. Am. Chem. Soc.* **2004**, *126*, 6972−6986.
(100) Noodleman, L.; Case, D. A.; Aizman, A. Broken symmetry analysis of spin coupling in iron-sulfur clusters. *J. Am. Chem. Soc.* **1988**, *110*, 1001−1005.
(101) Belorizky, E.; Fries, P. H. Exact solutions for simple spin clusters with isotropic Heisenberg exchange interactions. *J. Chim. Phys.* **1993**, *90*, 1077−1100.
(102) Sinn, E. Magnetic exchange in polynuclear metal complexes. *Coord. Chem. Rev.* **1970**, *5*, 313−347.

DOI: 10.1021/acs.jctc.9b00563
J. Chem. Theory Comput. 2019, 15, 5998−6009